Performance Enhancement by Tandem Wings Interaction of CoFlow Jet Aircraft

Yan Ren [*]   Gecheng Zha [†]
Coral Gables, FL 33124
Dept. of Mechanical and Aerospace Engineering
University of Miami, Coral Gables, Florida 33124

Abstract

This paper numerically studies the cruise efficiency enhancement by 3D tandem wings interaction for a CoFlow Jet (CFJ) aerial vehicle at cruise Mach number of 0.17. The simulations employ 3D RANS solver with Spalart-Allmaras (S-A) turbulence model, 3rd order WENO scheme for the inviscid fluxes, and 2nd order central differencing for the viscous terms. The aerodynamic performance, energy expenditure, and flow field of the tandem wing propeller-CFJ aircraft are investigated. Each of the tandem wings has a propeller mounted above the wing suction surface to reduce the CFJ power required. The front wing is smaller with the planform area 1/3 of that of the rear wing. Both wings have the same chord. The aspect ratio for the front wing is 3.56 and 10.68 for the rear wing. The area averaged aspect ratio of the aircraft is 8.9. The study holds a constant optimal angle of attack (AoA) of 5° for the front wing and has the AoA of the rear wing at 5°, 10°, and 15°. The two wings are separated by one chord length in the stream-wise direction and are aligned in the same transverse position. Such a configuration allows the rear wing to capture the tip vortex of the front wing on the suction surface with its low pressure. This vortex capturing mechanism enhances the lift of the rear wing significantly attributed to the low pressure of the tip vortex core and the upwash the vortex generates.

The optimal aerodynamic efficiency and productivity efficiency of the tandem wing vehicle system are obtained when the AoA of the rear wing is at 10°. When the AoA of the rear wing is increased from 5° to 10°, the increased circulation of the larger rear wing dominates the flow field. The induced circulation of the rear wing with a stronger propeller strength create an upwash favorable to the front wing, which produces an aerodynamic ratio of C_L/C_D of 21.85 and the corrected aerodynamic efficiency $C_L/(C_D)_c$ of 14.39. These are extraordinarily high merit results for the small front wing with a small aspect ratio of 3.56. The corrected aerodynamic efficiency $C_L/(C_D)_c$ for the whole vehicle is 14.27 with a lift coefficient of 1.6, which result in a corrected productivity efficiency $C_L^2/(C_D)_c$ for the whole vehicle of 22.82. The overall vehicle efficiency are excellent due to the high vehicle cruise lift coefficient of 1.6 and corrected aerodynamic efficiency of 14.27 for a moderate aspect ratio of 8.9. The cruise lift coefficient of 1.6 attributed to the CFJ active flow control is almost 3 times greater than that of conventional subsonic aircraft, which would be stalled at such a high lift coefficient or severely penalized by its excessive drag. This study indicates that the two tandem wings benefit each other. The front wing tip vortex enhances the lift of the rear wing and the rear wing's high lift and circulation increase the front wing's efficiency due to the upwash. The tandem wing configuration presented in this paper is not optimized and could be a start for a new area of aircraft configuration design. More investigation will be also conducted to study the propeller strength effect.

Nomenclature

CFJ Co-flow jet

---

[*] Postdoc Researcher, Ph.D., AIAA member
[†] Professor, AIAA Associate Fellow, Professor of the University of Miami

V	Flow Velocity
ρ	Air Density
α, AoA	Angle of Attack
$\dot{m}$	Mass Flow Rate
M	Mach Number
M_i	Isentropic Mach Number
Re	Reynolds Number
L	Aerodynamics Lift
D	Aerodynamic Drag
p	Static Pressure
p_0	Total Pressure
η	Pumping Power
q_∞	Freestream Dynamic Head, $\frac{1}{2}\rho_\infty V_\infty{}^2$
C_L	Lift Coefficient, $\frac{L}{q_\infty S}$
C_D	Drag Coefficient, $\frac{D}{q_\infty S}$
C_M	Moment Coefficient, $\frac{M}{q_\infty S c}$
C_p	Pressure Coefficient, $\frac{p-p_\infty}{q_\infty}$
C_μ	Jet Momentum Coefficient, $\frac{\dot{m}_j v_j}{q_\infty S}$
$(\frac{L}{D})$	Conventional Aerodynamic Efficiency
P_c	CFJ Power Coefficient, $\frac{P}{q_\infty S V_\infty}$
$(\frac{L}{D})_c$	Corrected Aerodynamic Efficiency for CFJ Airfoil, $\frac{L}{D+P/V_\infty} = \frac{C_L}{C_D+P_c}$
$(\frac{C_L^2}{C_D})$	Productivity Efficiency Coefficient
$(\frac{C_L^2}{C_D})_c$	Corrected Productivity Efficiency Coefficient for CFJ Airfoil
∞	Free Stream Conditions

1   Introduction

In nature, tandem wing configuration is widely adopted by insects, such as dragonflies and locusts. It is proven that such configuration could lead to superior stability and maneuverability, and could benefit the aerodynamic performance via active wing-wing interaction.

Tandem wing configuration has attracted a lot of interest recently due to the development of electric vertical takeoff/landing (VTOL) vehicles for urban air mobility[1, 2, 3]. The advantage of tandem wings is that it has high hovering stability due to two lifting vectors. However, it reduces the aircraft effective aspect ratio and the front wing's tip vortex and wake may affect the performance of the rear wing at cruise. How to optimize the tandem wing configuration to improve cruise efficiency is thus a very important topic, which is the purpose of this paper.

The rear wing of tandem wing aircraft often locates above the front wing to avoid the wake of the front wing and the propeller, which is perceived to be harmful to the aerodynamic performance. However, with the help of the advanced Co-Flow Jet (CFJ) flow control[4, 5, 6, 7, 8, 9, 10, 11, 12, 13, 14], the rear wing may benefit from the the incoming wake to improve the cruise efficiency as observed by the 2D study of Ren and Zha [15]. The CFJ wings for VTOL hover and cruise are also studied in [2, 3].

In this work, we take a 3D tandem wing propeller-CFJ VTOL vehicle as the model to study the tandem wings interaction effect at cruise. The tandem wing vehicle is an integrated flight system with front and rear CFJ

wings, each has propellers mounted above the wing suction surface as shown in Fig. 1. Following the same strategy developed by Ren and Zha [15], the tandem wings utilize the CFJ active flow control to enhance the cruise performance. Three cases with different rear wing angle of attack are studied for its effect on the overall aerodynamic performance. Also, the wing tip vortex capture mechanism is discussed for optimizing the airplane performance.
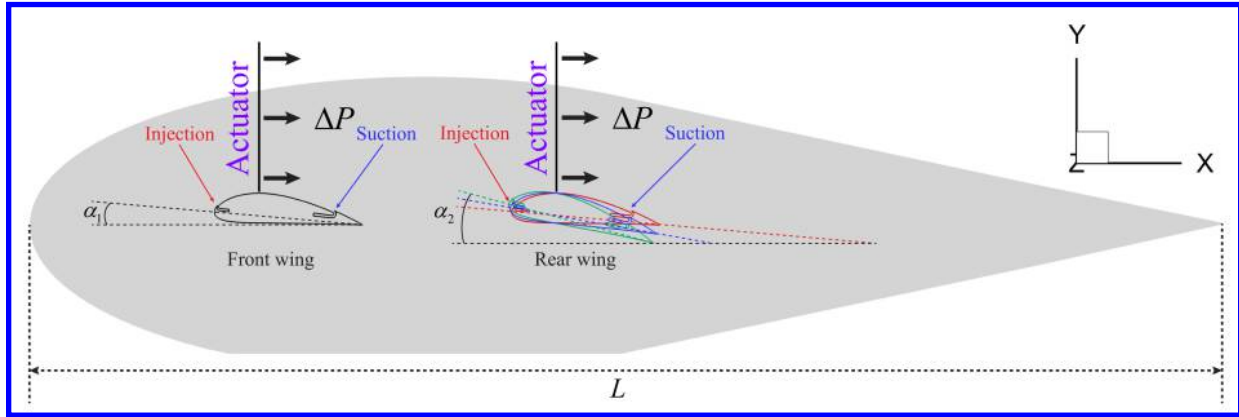

Figure 1: Side view of the tandem wing air vehicle with propellers mounted above the wings.

2   The Co-Flow Jet Active Flow Control Airfoil

The CFJ airfoil has an injection slot near the leading edge(LE) and a suction slot near the trailing edge(TE) on the airfoil suction surface as sketched in Fig. 2. A small amount of mass flow is withdrawn into the airfoil near the TE, pressurized and energized by a micro-compressor system inside the airfoil, and then injected near the LE in the direction tangent to the main flow. The whole process does not add any mass flow to the system and hence is a zero-net mass-flux flow control.

The CFJ airfoil flow control mechanism achieves a radical lift augmentation, drag reduction and stall margin increase at a very low energy expenditure. It can not only achieve ultra-high lift coefficient, but also significantly enhance cruise productivity efficiency and cruise wing loading from subsonic to transonic conditions[16, 17, 18, 19, 20, 21].

Yang and Zha [20] discovered in 2017 that a CFJ airfoil can achieve Super-Lift Coefficient(SLC), which is a lift coefficient that exceeds the theoretical limit of potential flow developed by Smith[22] and is defined below:

$$C_{Lmax} = 2\pi(1 + \frac{t}{c})$$ (1)

When a SLC occurs, the circulation is so high that the stagnation point is detached from the airfoil body as shown in Fig. 3, which has a C_{Lmax} of 10.6, far greater than the theoretical limit of 7.6. The freestream condition has a Mach number of 0.063 and Reynolds number of 3 million. The flow remains attached at AoA of 70° and the wake is filled with reversed velocity deficit, similar to the owl effect that generates very low wake turbulent noise. The CFJ airfoil pressure coefficient at the leading edge suction peak is nearly 10 times higher than the maximum value of the baseline airfoil at AoA of 18° before it stalls [20]. In other words, the CFJ airfoil at SLC condition can keep flow attached despite an adverse pressure gradient nearly one order of magnitude higher than the conventional airfoil. The simulation of Yang and Zha [20] also reveals a complex phenomenon with 4 layers of
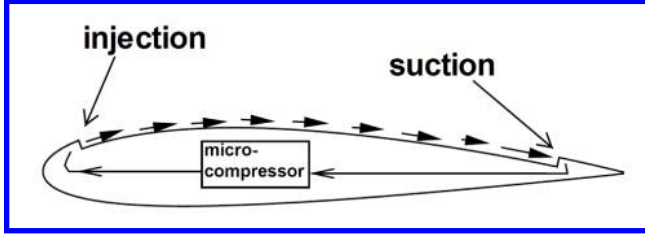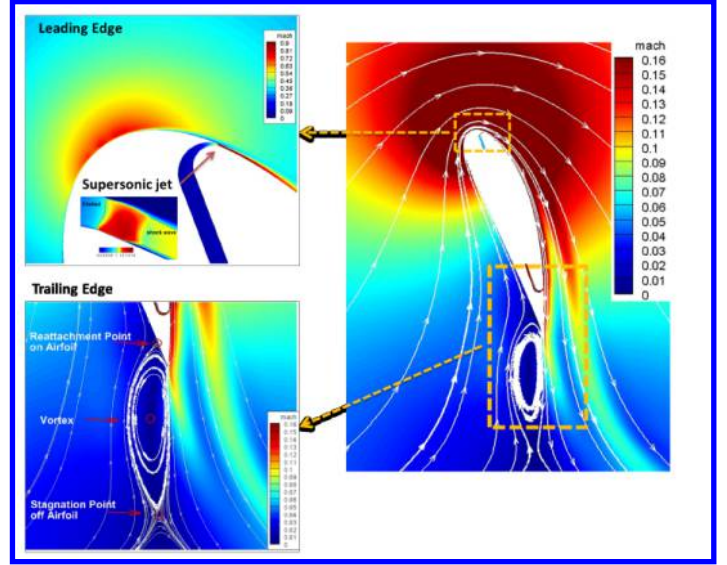
Figure 3: Mach number contours and streamlines at $C_\mu = 0.35$ and AoA $=70°$ for the CFJ6421-SST016-SUC053-INJ009 airfoil.

Figure 2: Baseline airfoil and CFJ Airfoil.

counter-rotating vortex layers emanating from leading edge and trailing to the wake of the airfoil. The detailed analysis can be seen in [20, 23].

3   Methodology

3.1   Tandem Wing Propeller-CFJ Parameters

The parameters used to define the tandem wing propeller-CFJ system are described in this section.

The injection jet momentum coefficient C_μ is used to describe the CFJ strength as:

$$C_\mu = \frac{\dot{m}V_j}{\frac{1}{2}\rho_\infty V_\infty{}^2 S} \tag{2}$$

where $\dot{m}$ is the injection mass flow, V_j is the mass-averaged injection velocity, ρ_∞ and V_∞ denote the free stream density and velocity, and S is the airfoil planform area.

The conventional airfoil aerodynamic efficiency is defined as

$$\left(\frac{L}{D}\right) = \frac{C_L}{C_D} \tag{3}$$

For CFJ wing, the ratio above represents the pure aerodynamic relationship between lift and drag. Taking into account the energy consumption of the CFJ, the conventional aerodynamic efficiency is modified by converting the power consumption into a corresponding drag force. The equation of the corrected aerodynamic efficiency is given as the following[18]

$$\left(\frac{L}{D}\right)_c = \frac{L}{D + \frac{P}{V_\infty}} \tag{4}$$

in which the CFJ pumping power consumption P is converted into a force $\frac{P}{V_\infty}$ added to the aerodynamic drag D. The formulation above can be further expressed using the non-dimensional coefficients C_L, C_D and P_c as

$$(\frac{C_L}{C_D})_c = \frac{C_L}{C_D + P_c} \tag{5}$$

Note that when the pumping power is set to 0, $(\frac{L}{D})_c$ returns to conventional aerodynamic efficiency definition. The C_L and C_D calculation needs to include the CFJ reactionary force as described by Zha et al [5].

The CFJ power required is determined by the total enthalpy rise from the suction duct outlet to the injection duct inlet[18]. The total enthalpy rise can be achieved by the embedded micro-compressors. The power required by the CFJ (P) can be expressed as:

$$P = \frac{\dot{m}H_{t2}}{\eta}(\Gamma^{\frac{\gamma-1}{\gamma}} - 1) \tag{6}$$

where γ is the specific heat ratio, Γ the total pressure ratio of the micro-compressor, H_{t2} the total enthalpy at the compressor inlet, $\dot{m}$ the jet mass flow rate, η the micro-compressor efficiency and is taken at 100% to compute the required power.

Eq. (6) indicates that the power required for CFJ is linearly determined by the mass flow rate and exponentially by the total pressure ratio. This relationship in fact applies to all the active flow controls based on fluidic actuators. Thus, C_μ should not be used to represent the power consumption of active flow control[18, 24]. For example, a high C_μ could have a substantially lower power consumption than a smaller C_μ if the high C_μ is created by a large mass flow rate and low jet velocity, which needs a significantly lower total pressure ratio[24, 25]. Yang and Zha[20] find that the only parameter correlated well with the maximum lift coefficient of CFJ airfoil is the power coefficient defined below:

$$P_c = \frac{P}{\frac{1}{2}\rho_\infty V_\infty^3 S} \tag{7}$$

where P is the CFJ required power defined in Eq. 6.

The transportation capability of an airplane is measured by how much total weight the aircraft can move for the maximum distance. In Yang et. al (2017)[20], a term "productivity" is defined as the product of the total weight by the maximum range to represent the transportation capability of an airplane.

For a jet engine airplane, the total weight of the aircraft decreases during flight. A non-dimensional productivity parameter is hence defined using the aircraft averaged weight as below:

$$C_{RW} = \frac{R\overline{W}}{\frac{1}{2c_t}\bar{\rho}V_\infty^3 S} = \frac{C_L^2}{C_D} \ln \frac{W_0}{W_f} \tag{8}$$

where R is the aircraft range, $\overline{W}$ is the averaged weight of the aircraft during cruise, c_t is the engine cruise thrust specific fuel consumption[fuel weight(N)/(thrust(N) s)], $\bar{\rho}$ is the averaged air density during cruise due to altitude variation, S is the wing platform area, W_0 is the aircraft initial gross weight at takeoff, W_f is the final weight at landing. This formulation is obtained from the Breguet Range Equation. The productivity parameter represents the productivity of the aircraft with the fuel consumed per unit time.

For a full electric battery powered propeller airplane, the aircraft weight will not change during flight. The productivity parameter is defined as:

$$C_{RW} = \frac{RW}{\frac{1}{2}\rho V_\infty^2 S E_c/g} = \eta \frac{C_L^2}{C_D} \frac{W_b}{W_0} \tag{9}$$

where E_c is the battery specific energy density (Wh/kg), W_b is the total battery weight, W_0 is the gross weight, η is the propulsion system efficiency (e.g. propeller).

Clearly, both Eq. (8) and (9) indicate that the productivity parameter is determined by C_L^2/C_D, which is thus defined as productivity efficiency. The productivity efficiency is considered as a more comprehensive parameter than the conventional aerodynamic efficiency C_L/C_D to measure the merit of an airplane aerodynamic design for cruise performance. The former includes not only the information of C_L/C_D, but also the information of the aircraft weight represented by C_L.

For CFJ airfoil, the productivity efficiency should also include the CFJ power consumption and is defined as below:

$$\frac{C_L^2}{C_{Dc}} = \frac{C_L^2}{C_D + P_C} \tag{10}$$

This study involves a tandem wing configuration. For example, the coefficient of lift for each wing can be defined individually as:

$$C_{L1} = \frac{L_1}{\frac{1}{2}\rho_\infty V_\infty^2 S_1}, \quad C_{L2} = \frac{L_2}{\frac{1}{2}\rho_\infty V_\infty^2 S_2}, \tag{11}$$

where the subscript 1 and 2 stand for the first and second wing. For the aircraft system with tandem wings, the system lift coefficient is defined as the total lift based on the total wing area below:

$$C_{Lt} = \frac{L_1 + L_2}{\frac{1}{2}\rho_\infty V_\infty^2 (S_1 + S_2)} \tag{12}$$

where the subscript t stands for tandem wing.

Substituting Eq. (11) to Eq. (12), the system lift coefficient can be expressed as:

$$C_{Lt} = \frac{C_{L1}S_1 + C_{L2}S_2}{S_1 + S_2} \tag{13}$$

Eq. (13) is actually the same as the area weighted lift coefficient. Similarly, the coefficient of system drag and CFJ power can be defined as:

$$C_{Dt} = \frac{C_{D1}S_1 + C_{D2}S_2}{S_1 + S_2} \tag{14}$$

$$P_{ct} = \frac{P_{c1}S_1 + P_{c2}S_2}{S_1 + S_2} \tag{15}$$

The corrected drag coefficient is:

$$(C_{Dc})_t = C_{Dt} + P_{ct} \tag{16}$$

The aerodynamic efficiency and the productivity efficiency of the tandem wing system then can be defined following the same way as Eq. (5) and Eq. (10). To see the relations clearly, we take the aerodynamic efficiency of the tandem wing as an example below:

$$(\frac{L}{D_c})_t = \frac{L_1 + L_2}{D_1 + D_2 + P_1/V_\infty + P_2/V_\infty} = \frac{C_{Lt}\frac{1}{2}\rho_\infty V_\infty^2(S_1 + S_2)}{C_{Dt}\frac{1}{2}\rho_\infty V_\infty^2(S_1 + S_2) + P_{ct}\frac{1}{2}\rho_\infty V_\infty^2(S_1 + S_2)}$$

$$= \frac{S_1 C_{L1} + S_2 C_{L2}}{S_1 C_{D1} + S_2 C_{D2} + S_1 P_{c1} + S_2 P_{c2}} \tag{17}$$

That is:

$$(\frac{L}{D_c})_t = \frac{C_{Lt}}{(C_{Dc})_t} \tag{18}$$

3.2 CFD Simulation Setup

The in house FASIP (Flow-Acoustics-Structure Interaction Package) CFD code is used to conduct the numerical simulation. The simulations employ 3D RANS solver with Spalart-Allmaras (S-A) turbulence model. A 3rd order WENO scheme for the inviscid flux [26, 27, 28, 29, 30, 31] and a 2nd order central differencing for the viscous terms [26, 30] are employed to discretize the Navier-Stokes equations. The low diffusion E-CUSP scheme used as the approximate Riemann solver suggested by Zha et al [27] is utilized with the WENO scheme to evaluate the inviscid fluxes. Implicit time marching method using Gauss-Seidel line relaxation is used to achieve a fast convergence rate [32]. Parallel computing is implemented to save wall clock simulation time [33].

3.3 Boundary Conditions

The 3rd order accuracy no slip condition is enforced on the solid surface with the wall treatment suggested in [34] to achieve the flux conservation on the wall. The computational mesh is shown in Fig. 4. Total pressure, total temperature and flow angles are specified at the CFJ injection duct inlet, as well as the upstream portion of the far field. Constant static pressure is applied at the suction duct outlet as well as the downstream portion of the far field. The total mesh size is about 10 million, split into 205 blocks for the parallel computation. The computational domain is about 150 chords in the main stream direction and 50 chords in wing span direction to ensure an accurate simulation. The first grid point on the wing surface is placed at $y^+ \approx 1$. The propeller is simulated using an actuator disk boundary condition with a pressure jump (ΔP) imposed. The pressure jump is given as a percentage of the pressure upstream of the actuator, typically is fairly small and rarely greater than 2%. The pressure jump condition is very well handled by the Riemann solver employed in the FASIP CFD code. In this study, the ΔP for each propeller actuator disk is iterated to make the system resultant force in the flight direction to be zero for the cruise condition.
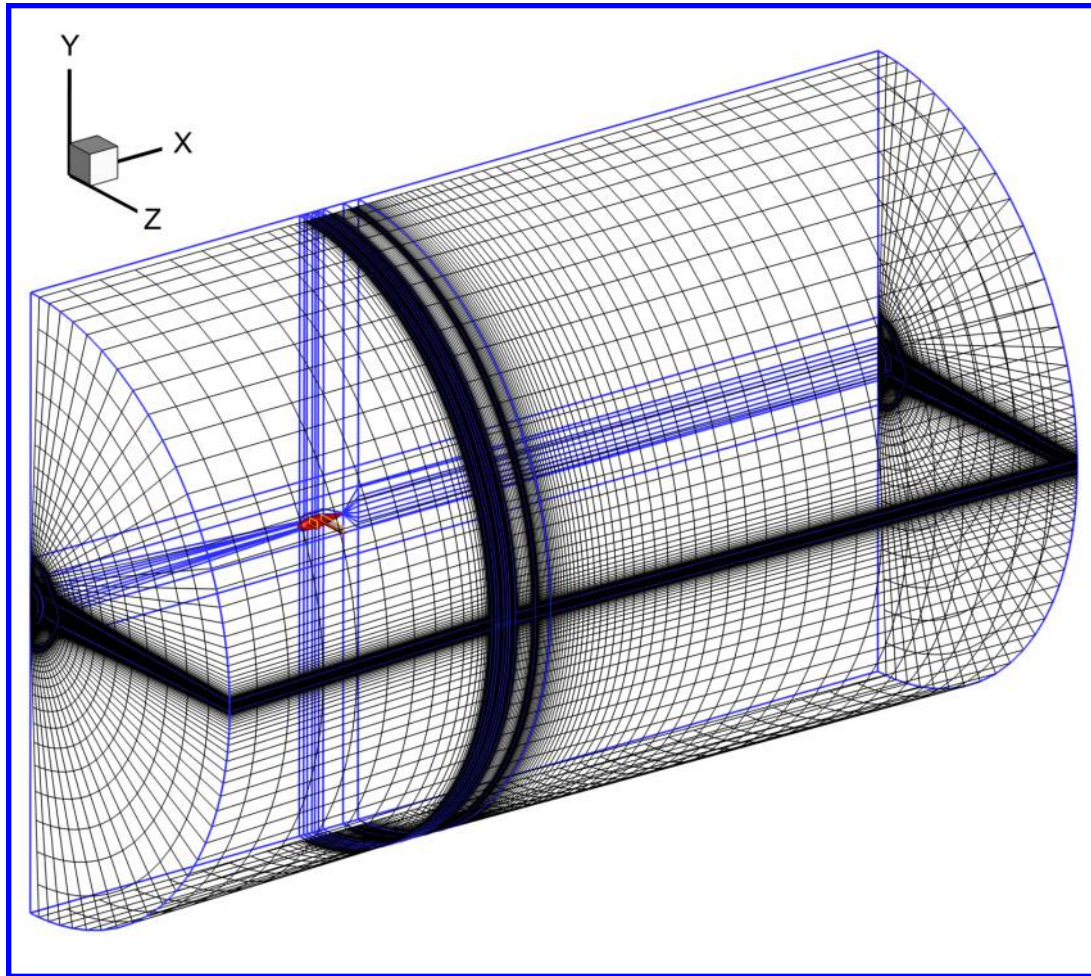
Figure 4: Computational mesh used in the current work.

4 Results and Discussion

Three cases (C1, C2, and C3) with different rear wing angle of attack α_2 are simulated first to study it's effect on the aerodynamic performance. The tandem wing aircraft wing tip vortex capture mechanism is discussed after in detail to optimize the airplane system efficiency.

The vehicle is a 4-seat tailless VTOL airplane for urban transportation with tandem wing configuration (Fig. 5). The simulation parameters are listed in Table 1. The two wings have the same chord length of 0.75m. As shown in Fig. 5 and Table 1, the rear wing is located at the same position as the front wing vertically, and 1C behind the front wing horizontally. The aspect ratios of the front wing and rear wing are 3.56 and 10.68, respectively. The aspect ratio of the aircraft is 8.9 based on the wing area weighted average [3]. The momentum coefficient $C_\mu = 0.04$ is used for both wings. The propeller strength is quantified by ΔP, and is iterated through out the simulation to obtain a zero net thrust cruise condition.

The free stream Mach number is 0.17 and the Reynolds number based on the wing chord is 1.07 million. the propeller actuator disks are normal to the free stream and are simulated as rectangular actuator disks to mimic a series of propellers that are placed next to each other. The propeller actuators are located on the top of the airfoil,

downstream of the injection slot and above the suction surface. This propeller position is optimized to interact with the CFJ airfoil to maximize the power efficiency for both VTOL hovering and cruise [2, 3, 15]. The airfoil used in the current study is the CFJ-NACA-6421 airfoil optimized by Wang and Zha[24, 25, 35].
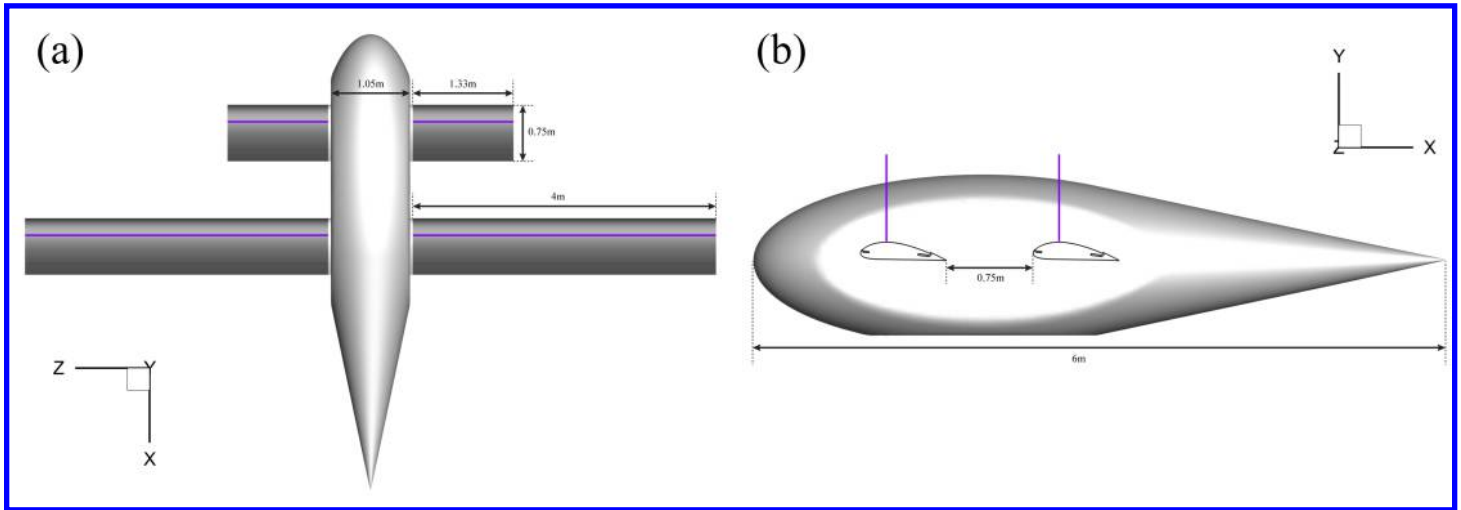

Figure 5: The top view (a) and side view (b) of the propeller-CFJ aircraft in the current study.

Table 1: Simulation parameters used in the current work.

Case	Items	AR	α	ΔP	M_∞	C_μ
C1	Front wing	3.56	5°	0.1288%	0.17	0.04
	Rear wing	10.68	5°			
	Full aircraft	8.9	-			
C2	Front wing	3.56	5°	0.2031%	0.17	0.04
	Rear wing	10.68	10°			
	Full aircraft	8.9	-			
C3	Front wing	3.56	5°	0.3379%	0.17	0.04
	Rear wing	10.68	15°			
	Full aircraft	8.9	-			

4.1 The effect of rear wing angle of attack

As mentioned before, the effect of rear wing angle of attack on the aerodynamic performance is investigated in this section. Three cases, case C1, C2, and C3 with the rear wing angle of attack 5°, 10°, and 15° are investigated with the front wing AoA fixed at 5°.

Fig. 6 (a), (c), and (e) show the vorticity iso-surface wake structures and streamlines of the three cases. The wing tip vortices of the front wing and rear wing are well identified by the roll-up vortex tubes trailing from the wing tips. The rear wing tip vortex become stronger as the α_2 increase and generates a higher lift coefficient. It is very clear that the front wing tip vortex propagate to downstream and interact with the rear wing. For case C1 and C2, the front wing tip vortex firmly attaches to the rear wing suction surface. However, for case C3, the front wing tip vortex is lifted off the rear wing suction surface due to the high angle of attack.
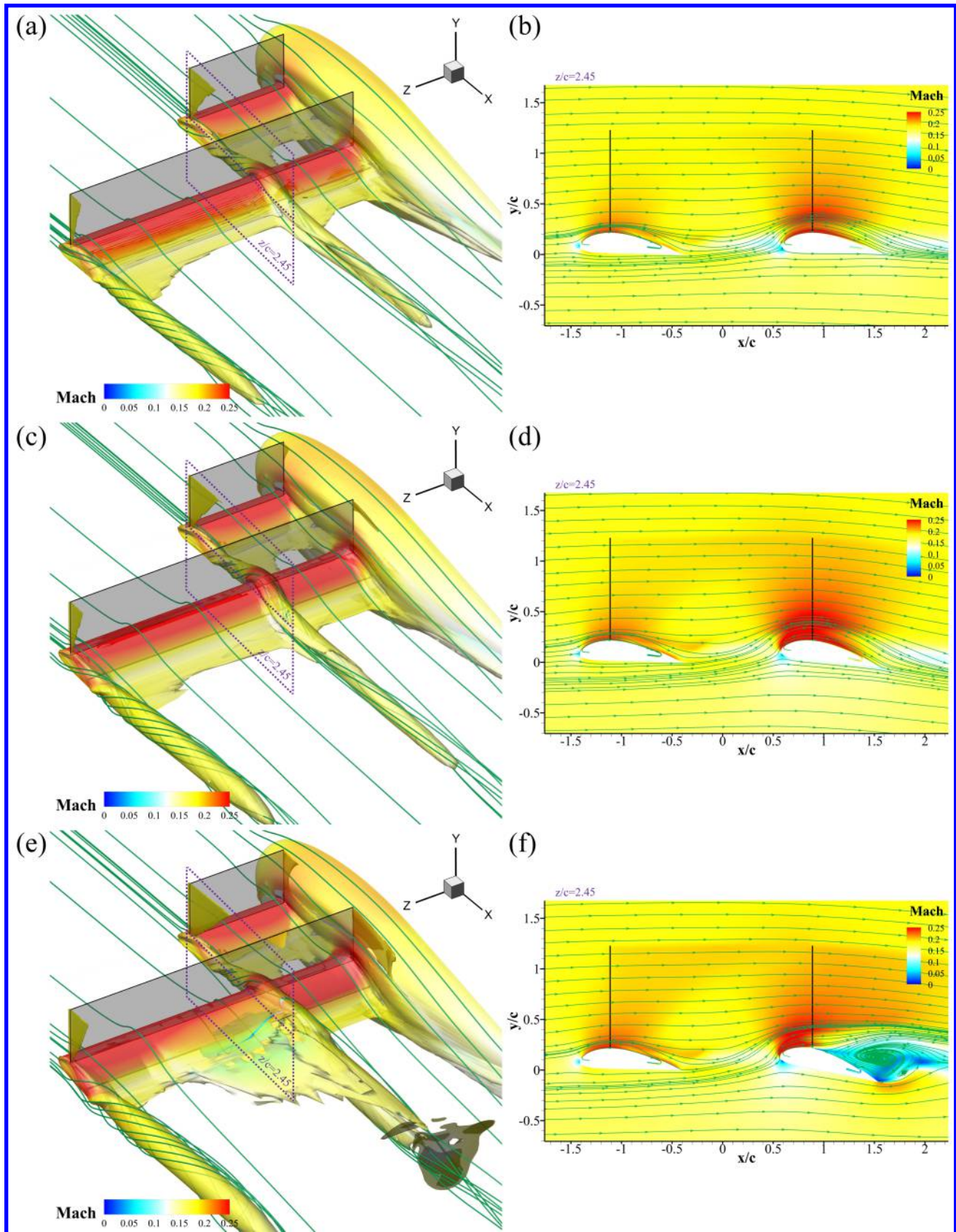
Figure 6: The wake structures represented by the vorticity iso-surface (colored by Mach nubmer) and streamlines of the case C1 (a), C2 (c), and C3 (e); Flow slice Mach contours at z/c=2.45 (front wing tip region) for the case C1 (b), C2 (d), and C3 (f).

Fig. 6 (b), (d), and (f) show the flow field Mach contours with streamlines at z/c=2.45 span section, which is the location that the front wing tip vortex strikes the rear wing. The front wing tip vortex is lifted upward by the low pressure of the rear wing suction surface and creates an upwash effect for both the front and the rear wing. The higher the rear wing AoA, the stronger the upwash effect, which can be also interpreted as being induced by the circulation of the rear wing. Both the upper mounted propellers and CFJ at C_μ of 0.04 are beneficial to attach the flow up to AoA of 10° for the rear wing. For the AoA of 15° of the rear wing, the rear wing is not able to attach the flow due to the high adverse pressure gradient caused by its own high AoA and the upwash of the front wing tip vortex. The flow is expected to be attached if the C_μ is further increased. But it may not be necessarily optimal from the aircraft system efficiency point of view.

Table 2 lists the quantitative aerodynamic performance of the three cases. For the case C1, the rear wing aerodynamic efficiency and productivity efficiency are much better than those of the front wing due to the larger wing aspect ratio and the wing tip vortex capture shown in Fig. 6. The corrected aerodynamic efficiency in terms of $C_L/(C_D)_c$ is 11.67 for the front wing and is 16.87 for the rear wing. The corrected productivity efficiency $C_L^2/(C_D)_c$ is 10.90 for the front wing and is 17.60 for the rear wing. The $C_L/(C_D)_c$ and $C_L^2/(C_D)_c$ for the full aircraft are 14.53 and 16.71, respectively.

Table 2: Aerodynamic performance of the tandem propeller-CFJ aircraft in the present study.

Case	Items	AR	C_L	C_D	P_c	C_L/C_D	$C_L/(C_D)_c$	$C_L^2/(C_D)_c$
C1	Fuselage	-	0.133	0.0127	-	-	-	-
	Front wing	3.56	0.934	0.0541	0.0259	17.26	11.67	10.90
	Rear wing	10.68	1.043	0.0380	0.0239	27.49	16.87	17.60
	Full aircraft	8.9	1.149	0.0547	0.0244	21.02	14.53	16.71
C2	Fuselage	-	0.188	0.0138	-	-	-	-
	Front wing	3.56	1.049	0.0480	0.0249	21.85	14.39	15.09
	Rear wing	10.68	1.533	0.0901	0.0166	17.00	14.35	22.00
	Full aircraft	8.9	1.599	0.0934	0.0187	17.12	14.27	22.82
C3	Fuselage	-	0.217	0.0162	-	-	-	-
	Front wing	3.56	1.105	0.0407	0.0243	27.14	16.99	18.78
	Rear wing	10.68	1.600	0.1819	0.0201	8.79	7.92	12.67
	Full aircraft	8.9	1.694	0.1627	0.0211	10.40	9.21	15.59

For the case C2 with the rear wing at AoA increased to 10°, the $C_L/(C_D)_c$ for the whole vehicle is 14.27, which is about the same as the case C1. The increased circulation of the rear wing due to the higher AoA increases the upwash of the front wing. Compared with case C1, the propeller strength is also increased by 57% to overcome the higher drag of the rear wing due to increased AoA. All these effects have the front wing's C_L increased, C_D decreased, and the CFJ P_c slightly reduced with the same C_μ of 0.04. They result in an increase of C_L/C_D by 26.6% and $C_L/(C_D)_c$ by 23.1% for the front wing compared with case C1. The rear wing C_L is substantially increased by 47% to 1.533 for Case C2 and the drag is increased by 137% attributed to the enlarged induced drag. But the CFJ P_c of the rear wing is decreased by 31% due to the stronger suction effect at leading edge of the CFJ airfoil at a higher AoA that requires less power to pump the mass flow. The $C_L/(C_D)_c$ for the rear wing is decreased by 14.9%. However, the corrected productivity efficiency $C_L^2/(C_D)_c$ for the whole airplane is 22.82 , and increase by 36.6% compared with the case C1. The productivity efficiency improvement from the front wing and rear wing are 38.4% and 25%, respectively. It suggests that higher AoA of the rear wing with 3 times larger area and aspect ratio than the front wing creates a circulation that dominates the whole tandem wing system.

The very interesting result is that the front wing with a small aspect ratio of 3.56 is able to achieve a aerodynamic

ratio of C_L/C_D of 21.85 and the corrected aerodynamic efficiency $C_L/(C_D)_c$ of 14.39. These are extraordinarily high merit results for such a small aspect ratio. As shown in Table 1, the propeller strength of Case C2 for both wings is increased by 57.7% compared to that of case C1 to overcome the increased drag of the rear wing caused by the high angle of attack. It is not clear at this point weather the front wing efficiency improvement is attributed to the overall circulation increase due to the rear wing high AoA or the stronger induction effect caused by the increased propeller strength. More study needs to be done to distinguish the effect.

For the case C3, the $C_L/(C_D)_c$ for the whole vehicle is 9.21, a decreases of 36.6% compared with the case C1. However, the front wing performance is further improved. The $C_L/(C_D)_c$ is increased by 45.6% and $C_L^2/(C_D)_c$ by 72.3% for the front wing comparing with the case C1. Similar to the Case C2, more investigation needs to be done to understand if the front wing efficiency improvement is because of the rear wing higher AoA, or the propeller strength increase. The rear wing performance is substantially decreased at AoA of 15° due to the large separation as shown in Fig. 6 (f).
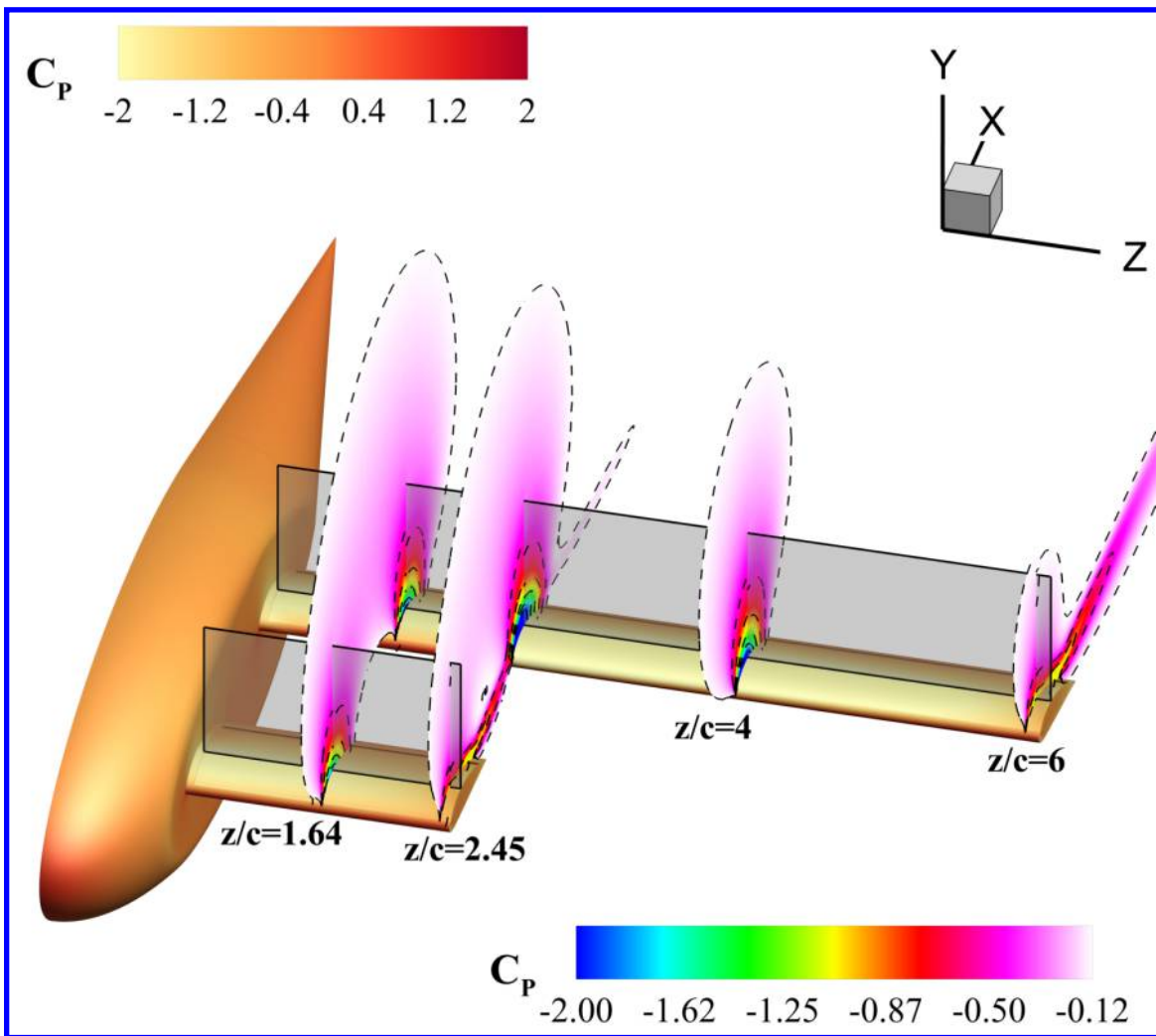

Figure 7: Flow slice C_p contours of the case C2 at z/c=1.64, 2.45, 4, and 6 along the wing span. The aircraft is colored by surface C_p

4.2 The effect of wing tip vortex capture

The results in last section show that a moderately high AoA for the rear CFJ wing with no separation is beneficial to the efficiency of the front CFJ wing and rear wing. This section is to conduct a more detailed analysis by examining the Case C2 that has the best system efficiency. Fig. 7 shows four static pressure field cross sections along the wing spans of the case C2. At z/c=1.64 (mid front wing), the rear wing low pressure region is greater than the front wing due to larger angle of attack. At z/c=2.45 (front wing tip region), the low pressure region of the front wing becomes smaller and the one for the rear wing is substantially larger, not just than the one in the front, also larger than those at inner and outer span locations. At z/c=4 and 6, the low pressure region gradually deceases with the airfoil load.

Fig. 8 shows the C_p distribution of the two wings at z/c=1.64 and 2.45. The discontinuity of the curves are due to the injection and suction slots of the CFJ airfoils. Fig.8 (a) shows that the C_p distribution of the two wings are similar on the pressure side, and the rear wing shows a much lower pressure on the suction side due to a higher angle of attack of the rear wing. At the front wing tip region (z/c=2.45, Fig. 8 b), the front wing load is substantially reduced compared with that at the inner span at z/c=1.64 due to the tip vortex effect. On the contrary, the rear wing load at this location is substantially greater than that at the inner span of z/c=1.64 because the rear wing captures the tip vortex of the front wing with a significant upwash with increased AoA, as shown in Fig. 6 (c) and (d).
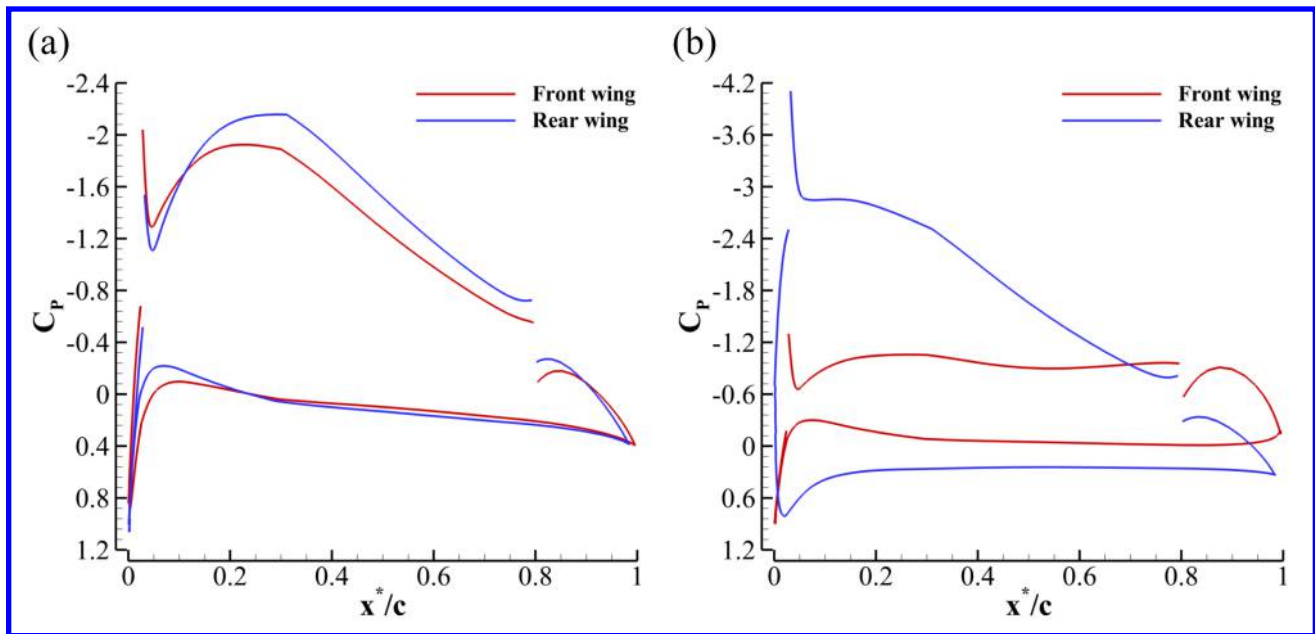

Figure 8: C_p distribution of the front wing and rear wing at z/c=1.64 (a) and 2.45 (b) of the case C2.

The C_p distribution of the rear wing at four wing span locations are plotted in Fig. 9 (a). The corresponding C_p surface integral along the wing span is plotted in Fig. 9 (b). Fig. 9 (a) shows that the surface pressure load of the rear wing along the span is sharply increased in the region capturing the front wing tip vortex due to two reasons: 1) the low pressure of the front wing tip vortex enhances the upper surface suction effect; 2) the upwash increases the AoA and further augment the effect. The CFJ wing plays a crucial role to maintain the flow attachment with the tip vortex capturing. Such a loading distribution is clearly shown again in Fig. 9 (b) that the peak of the curve corresponds to the location where the front wing tip vortex is captured by the rear wing.
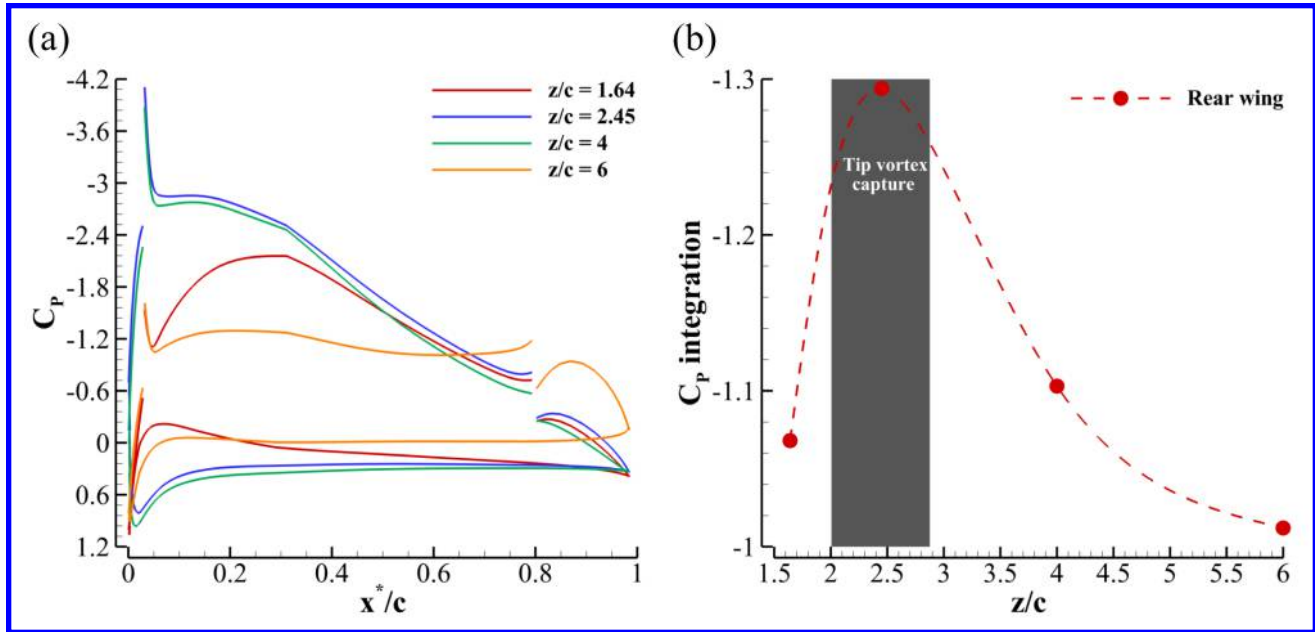
Figure 9: (a) C_p distribution of the rear wing at z/c=1.64, 2.45, 4, and 6 of the case C2; (b) C_p surface integration along the rear wing span for the case C2.

5   Conclusion

This paper numerically studies the cruise efficiency enhancement by 3D tandem wings interaction for a CoFlow Jet (CFJ) aerial vehicle at cruise Mach number of 0.17. The simulations employ 3D RANS solver with Spalart-Allmaras (S-A) turbulence model, 3rd order WENO scheme for the inviscid fluxes, and 2nd order central differencing for the viscous terms. The aerodynamic performance, energy expenditure, and flow field of the tandem wing propeller-CFJ aircraft are investigated. Each of the tandem wings has a propeller mounted above the wing suction surface to reduce the CFJ power required. The front wing is smaller with the planform area 1/3 of that of the rear wing. Both wings have the same chord. The aspect ratio for the front wing is 3.56 and 10.68 for the rear wing. The area averaged aspect ratio of the aircraft is 8.9. The study holds a constant optimal angle of attack (AoA) of 5° for the front wing and has the AoA of the rear wing at 5°, 10°, and 15°. The two wings are separated by one chord length in the stream-wise direction and are aligned in the same transverse position. Such a configuration allows the rear wing to capture the tip vortex of the front wing on the suction surface with its low pressure. This vortex capturing mechanism enhances the lift of the rear wing significantly attributed to the low pressure of the tip vortex core and the upwash the vortex generates.

The optimal aerodynamic efficiency and productivity efficiency of the tandem wing vehicle system are obtained when the AoA of the rear wing is at 10°. When the AoA of the rear wing is increased from 5° to 10°, the increased circulation of the larger rear wing dominates the flow field. The induced circulation of the rear wing with a stronger propeller strength create an upwash favorable to the front wing, which produces an aerodynamic ratio of C_L/C_D of 21.85 and the corrected aerodynamic efficiency $C_L/(C_D)_c$ of 14.39. These are extraordinarily high merit results for the small front wing with a small aspect ratio of 3.56. The corrected aerodynamic efficiency $C_L/(C_D)_c$ for the whole vehicle is 14.27 with a lift coefficient of 1.6, which result in a corrected productivity efficiency $C_L^2/(C_D)_c$ for the whole vehicle of 22.82. The overall vehicle efficiency are excellent due to the high vehicle cruise lift coefficient of 1.6 and corrected aerodynamic efficiency of 14.27 for a moderate aspect ratio of 8.9. The cruise lift coefficient

of 1.6 attributed to the CFJ active flow control is almost 3 times greater than that of conventional subsonic aircraft, which would be stalled at such a high lift coefficient or severely penalized by its excessive drag. This study indicates that the two tandem wings benefit each other. The front wing tip vortex enhances the lift of the rear wing and the rear wing's high lift and circulation increase the front wing's efficiency due to the upwash. The tandem wing configuration presented in this paper is not optimized and could be a start for a new area of aircraft configuration design. More investigation will be also conducted to study the propeller strength effect.

6   Acknowledgment

References

[1] Uber Elevate, "Fast-Forwarding to a Future of On-Demand Urban Air Transportation." Uber White Paper, Oct. 27, 2016.

[2] G.-C. Zha, Y. Ren, J.-Y. Gan, and D. Espinal, "A High Efficiency Low Noise VTOL/ESTOL Concept Using CoFLow Jet Airfoil." AIAA Paper 2019-4467, AIAA Propulsion and Energy 2019 Forum, Indianapolis, Indiana, 19-22 August 2019.

[3] J. Boling, Y. Ren, G.-C. Zha, and C. Zeune, " High Speed High Efficiency VTOL Aircraft Using CoFlow Jet Active Flow Control Wings." AIAA Paper 2020-2792, VIRTUAL EVENT AIAA AVIATION 2020 FORUM, 15-19 June, 2020.

[4] G.-C. Zha and D. C. Paxton, "A Novel Flow Control Method for Airfoil Performance Enhancement Using Co-Flow Jet." *Applications of Circulation Control Technologies*, Chapter 10, p. 293-314, Vol. 214, Progress in Astronautics and Aeronautics, AIAA Book Series, Editors: Joslin, R. D. and Jones, G.S., 2006.

[5] G.-C. Zha, W. Gao, and C. Paxton, "Jet Effects on Co-Flow Jet Airfoil Performance," *AIAA Journal, No. 6,*, vol. 45, pp. 1222–1231, 2007.

[6] G.-C. Zha, C. Paxton, A. Conley, A. Wells, and B. Carroll, "Effect of Injection Slot Size on High Performance Co-Flow Jet Airfoil," *AIAA Journal of Aircraft*, vol. 43, 2006.

[7] G.-C. Zha, B. Carroll, C. Paxton, A. Conley, and A. Wells, "High Performance Airfoil with Co-Flow Jet Flow Control," *AIAA Journal*, vol. 45, 2007.

[8] Wang, B.-Y. and Haddoukessouni, B. and Levy, J. and Zha, G.-C., "Numerical Investigations of Injection Slot Size Effect on the Performance of Co-Flow Jet Airfoil," *Journal of Aircraft*, vol. Vol. 45, No. 6,, pp. pp.2084–2091, 2008.

[9] B. P. E. Dano, D. Kirk, and G.-C. Zha, "Experimental Investigation of Jet Mixing Mechanism of Co- Flow Jet Airfoil." AIAA-2010-4421, 5th AIAA Flow Control Conference, Chicago, IL, 28 Jun - 1 Jul 2010.

[10] B. P. E. Dano, G.-C. Zha, and M. Castillo, "Experimental Study of Co-Flow Jet Airfoil Performance Enhancement Using Micro Discreet Jets." AIAA Paper 2011-0941, 49th AIAA Aerospace Sciences Meeting, Orlando, FL, 4-7 January 2011.

[11] A. Lefebvre, B. Dano, W. Bartow, M. Fronzo, and G. Zha, "Performance and energy expenditure of coflow jet airfoil with variation of mach number," *Journal of Aircraft*, vol. 53, no. 6, pp. 1757–1767, 2016.

[12] A. Lefebvre, G-C. Zha, "Numerical Simulation of Pitching Airfoil Performance Enhancement Using Co-Flow Jet Flow Control," *AIAA paper 2013-2517*, June 2013.

[13] A. Lefebvre, G-C. Zha, "Cow-Flow Jet Airfoil Trade Study Part I : Energy Consumption and Aerodynamic Performance," *32nd AIAA Applied Aerodynamics Conference, AIAA AVIATION Forum, AIAA 2014-2682*, June 2014.

[14] A. Lefebvre, G-C. Zha, "Cow-Flow Jet Airfoil Trade Study Part II : Moment and Drag," *32nd AIAA Applied Aerodynamics Conference, AIAA AVIATION Forum, AIAA 2014-2683*, June 2014.

[15] G.-C. Zha, Y. Ren, J.-Y. Gan, and D. Espinal, "High Efficiency Tandem Propeller-CoFlow Jet Airfoil System in Cruise." AIAA Paper 2020-2779, VIRTUAL EVENT AIAA AVIATION 2020 FORUM, 15-19 June 2020.

[16] Lefebvre, A. and Zha, G.-C. , "Design of High Wing Loading Compact Electric Airplane Utilizing Co-Flow Jet Flow Control." AIAA Paper 2015-0772, AIAA SciTech2015: 53nd Aerospace Sciences Meeting, Kissimmee, FL, 5-9 Jan 2015.

[17] Lefebvre, A. and Zha, G.-C., "Trade Study of 3D Co-Flow Jet Wing for Cruise and Takeoff/Landing Performance." AIAA Paper 2016-0570, AIAA SCITECH2016, AIAA Aerospace Science Meeting, San Diego, CA, 4-8 January 2016.

[18] Lefebvre, A. and Dano, B. and Bartow, W. and Di Franzo, M. and Zha, G.-C., "Performance Enhancement and Energy Expenditure of Co-Flow Jet Airfoil with Variation of Mach Number." AIAA Paper 2013-0490, AIAA Journal of Aircraft, DOI: 10.2514/1.C033113, 2016.

[19] Liu, Z.-X. and Zha, G.-C., "Transonic Airfoil Performance Enhancement Using Co-Flow Jet Active Flow Control." AIAA Paper 2016-3472, AIAA AVIATION 2016, 8th AIAA Flow Control Conference, Washington, D.C, June 13-17, 2016.

[20] Yang, Y.-C. and Zha, G.-C., "Super-Lift Coefficient of Active Flow Control Airfoil: What Is the Limit?." AIAA Paper 2017-1693, AIAA SCITECH2017, 55th AIAA Aerospace Science Meeting, Grapevine, Texas, 9-13 January 2017.

[21] G.-C. Zha, Y.-C. Yang, Y. Ren, and B. McBreen, "Super-lift and thrusting airfoil of coflow jet-actuated by micro-compressors." AIAA Paper 2017-3061, AIAA AVIATION 2018, Atlanta, GA , 25 - 29 June 2018.

[22] A. Smith, "High-Lift Aerodynamics," *Journal of Aircraft*, vol. 12, pp. 501–530, 1975.

[23] G.-C. Zha, "Estol performance for heavy lift transports using ultra-high lift high efficiency co-flow jet airfoil." Final Report to DARPA for Contract HR0011-16-2-0052, May 25, 2018.

[24] Y. Wang and G.-C. Zha, "Study of 3D Co-flow Jet Wing Induced Drag and Power Consumption at Cruise Conditions." AIAA Paper 2019-0034, AIAA SciTech 2019, San Diego, CA, January 7-11, 2019.

[25] Y. Wang, Y.-C. Yang, and G.-C. Zha, "Study of Super-Lift Coefficient of Co-Flow Jet Airfoil and Its Power Consumption." AIAA Paper 2019-3652, AIAA Aviation 2019, AIAA Applied Aerodynamics Conference, Dallas, Texas, 17-21 June 2019.

[26] Y.-Q. Shen and G.-C. Zha, "Large Eddy Simulation Using a New Set of Sixth Order Schemes for Compressible Viscous Terms ," *Journal of Computational Physics*, vol. 229, pp. 8296–8312, 2010.

[27] Zha, G.C., Shen, Y.Q. and Wang, B.Y., "An improved low diffusion E-CUSP upwind scheme ," *Journal of Computer and Fluids*, vol. 48, pp. 214–220, Sep. 2011.

[28] Y.-Q. Shen and G.-Z. Zha , "Generalized finite compact difference scheme for shock/complex flowfield interaction," *Journal of Computational Physics*, vol. doi:10.1016/j.jcp.2011.01.039, 2011.

[29] Shen, Y.-Q. and Zha, G.-C. and Wang, B.-Y., " Improvement of Stability and Accuracy of Implicit WENO Scheme," *AIAA Journal*, vol. 47, No. 2, pp. 331–344, 2009.

[30] Shen, Y.-Q. and Zha, G.-C. and Chen, X.-Y., " High Order Conservative Differencing for Viscous Terms and the Application to Vortex-Induced Vibration Flows," *Journal of Computational Physics*, vol. 228(2), pp. 8283–8300, 2009.

[31] Shen, Y.-Q. and Zha, G.-C. , " Improvement of the WENO Scheme Smoothness Estimator," *International Journal for Numerical Methods in Fluids*, vol. DOI:10.1002/fld.2186, 2009.

[32] G.-C. Zha and E. Bilgen, "Numerical Study of Three-Dimensional Transonic Flows Using Unfactored Upwind-Relaxation Sweeping Algorithm," *Journal of Computational Physics*, vol. 125, pp. 425–433, 1996.

[33] B.-Y. Wang and G.-C. Zha, "A General Sub-Domain Boundary Mapping Procedure For Structured Grid CFD Parallel Computation," *AIAA Journal of Aerospace Computing, Information, and Communication*, vol. 5, No.11, pp. 2084–2091, 2008.

[34] Y.-Q. Shen, G.-C. Zha, and B.-Y. Wang, "Improvement of Stability and Accuracy of Implicit WENO Scheme ," *AIAA Journal*, vol. 47, pp. 331–344, 2009.

[35] Y. Wang and G.-C. Zha, "Study of Mach Number Effect for 2D Co-Flow Jet Airfoil at Cruise Conditions." AIAA Paper 2019-3169, AIAA Aviation 2019, AIAA Applied Aerodynamics Conference, Dallas, Texas, 17-21 June 2019.